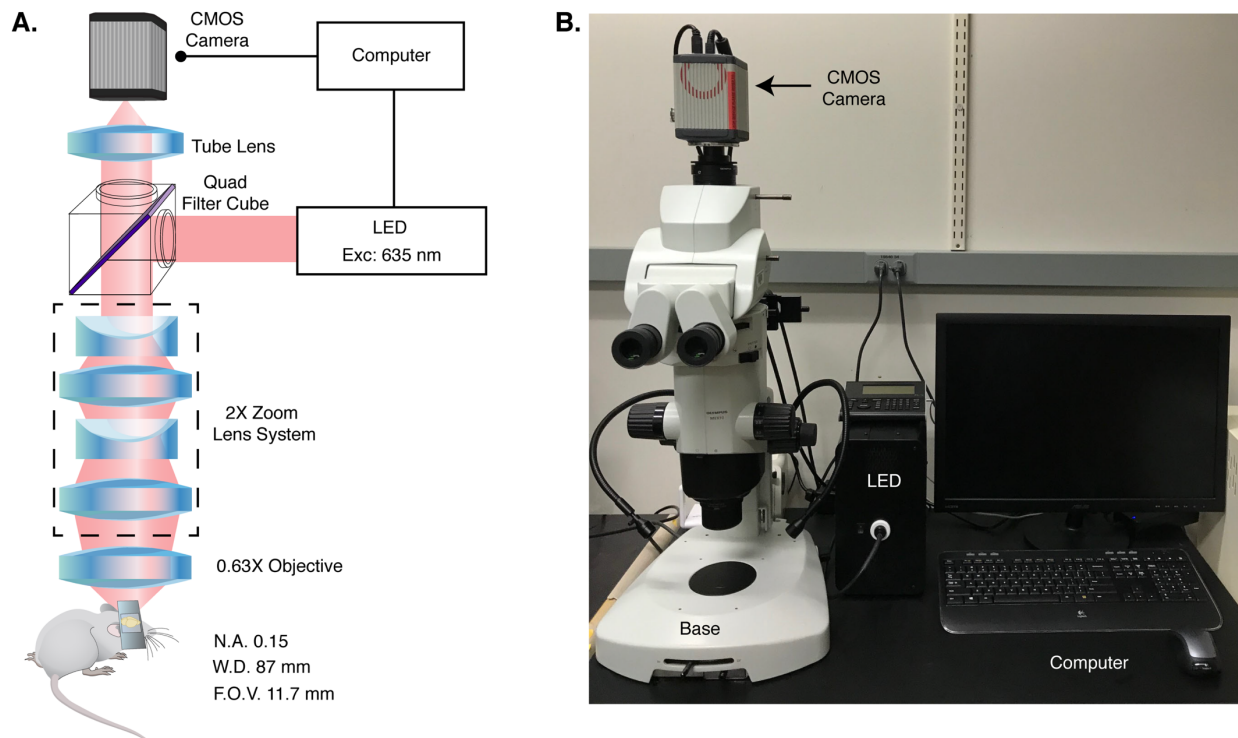
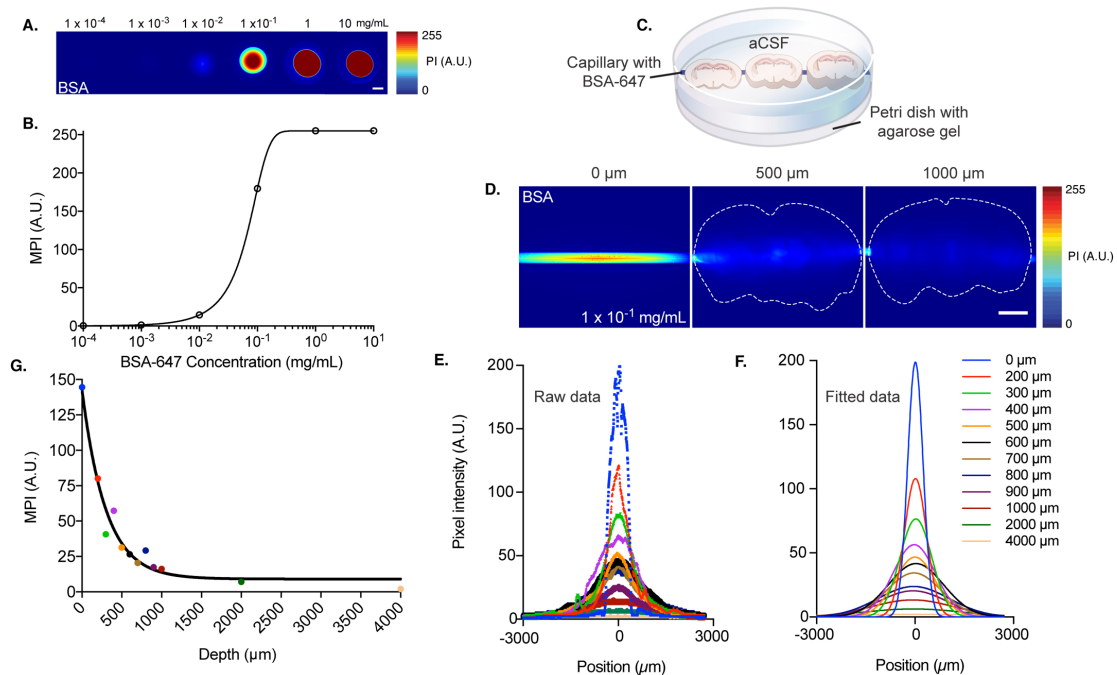


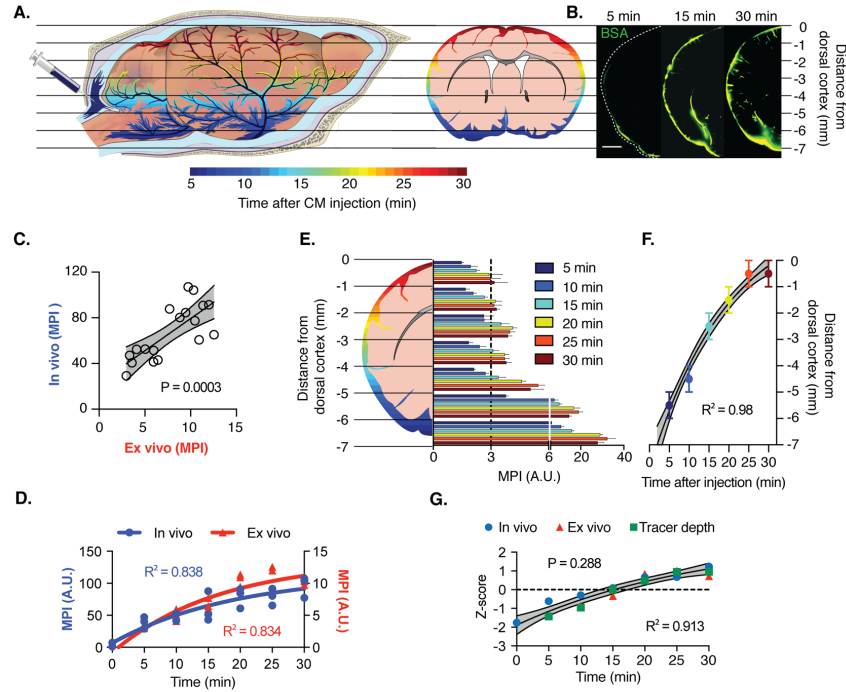
## Supplementary Figures



**Supplementary Figure 1. Transcranial macroscopic imaging system. (A)** Optical schematic. The system uses a tunable LED illumination system that allows individual control of up to 16 different wavelengths. Excitation for 647nm fluorophores was achieved using a 635 nm wavelength. The imaging software controls rapid switching between wavelengths and when paired with a quad filter cube enables high-speed 4 channel imaging (~100Hz) without having to rotate the filter turret. The macroscope has a total magnification of 4-40X and with a 0.63X objective permits a long working distance (W.D.) and a high numerical aperture (N.A.) with a field of view (F.O.V.) of about 11.7 mm at the magnification used for this study. This set-up uses a scientific CMOS camera that has an effective area of 13.312 x 13.312 mm and a full resolution of 2048 x 2048 pixels, enabling fast image acquisition (100 frames per second). The system is compatible with image splitting optics for simultaneous two-channel applications for dual CSF tracer studies. **(B)** Photograph of the macroscopic imaging system.

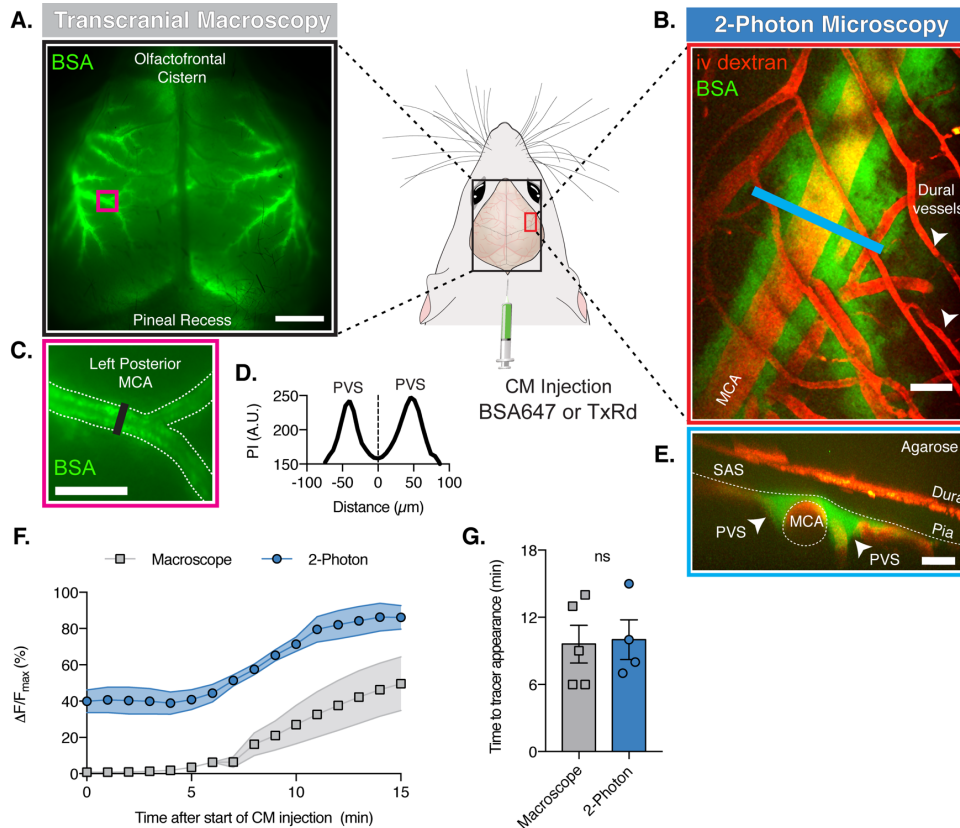


**Supplementary Figure 2. Imaging penetration depth analysis.** (A) Bovine serum albumin-conjugated to AlexaFluor 647 (BSA) was serially diluted from  $10$  to  $1 \times 10^{-4}$  mg/mL in artificial CSF (aCSF). A  $10 \mu\text{l}$  drop was aliquoted into a 96-well plate and imaged on the macroscope at a  $635$  nm wavelength using the same magnification and exposure time used in the in vivo experiments. Images were color-coded for pixel intensity (PI) in arbitrary units (A.U.) from  $0$  to  $255$  (scale bar =  $2$  mm). (B) Mean pixel intensity (MPI) was calculated for each  $10 \mu\text{l}$  droplet and plotted as a function of tracer concentration. The data was fit with a variable slope sigmoidal function. The optimal dilution of tracer that is within the range of the in vivo experiments was  $0.1$  mg/ml. (C) Schematic of the experimental set-up showing acute coronal sections of increasing thickness placed over a capillary filled with BSA-647 embedded in agar. (D) Representative PI color-coded images of the fluorescent capillary in the plane of focus with: no tissue ( $0 \mu\text{m}$ ), a  $500 \mu\text{m}$ -thick, and  $1,000 \mu\text{m}$ -thick coronal section placed above the capillary (scale bar =  $2$  mm). (E) Raw PI from  $6000 \mu\text{m}$  line scans centered over the capillary acquired through coronal sections of increasing thickness between  $200$ - $4000 \mu\text{m}$ . (F) Gaussian fit of the raw data from (E) showed good agreement for all ( $R^2 > 0.924$ ) except the  $4,000 \mu\text{m}$  ( $R^2 = 0.55$ ). (G) Regions of interest were drawn over the capillary within the perimeter of the coronal section and MPI was measured and plotted as a function of depth. Data was fit using a one phase exponential decay function ( $R^2 = 0.96$ ) showing that fluorescent signal plateaus between  $1$ - $2$  mm of tissue thickness, in agreement with results from (F).

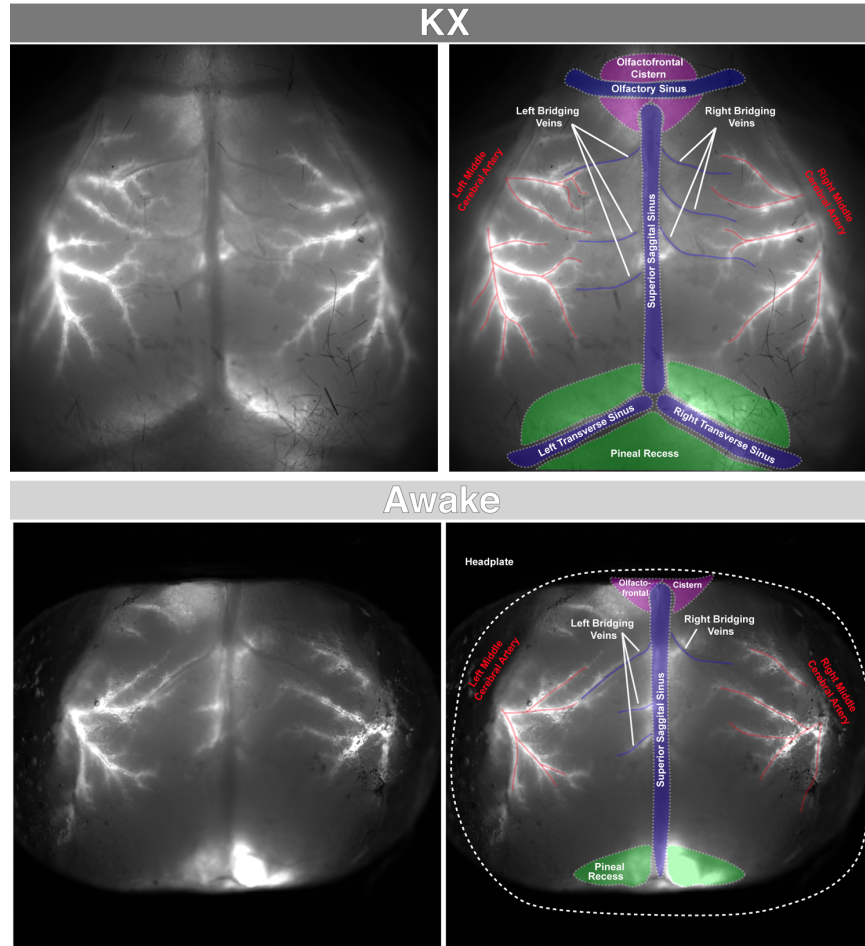


**Supplementary Figure 3. In vivo transcranial imaging correlates with tracer transport to the dorsal cortex and ex vivo quantification at all timepoints.**

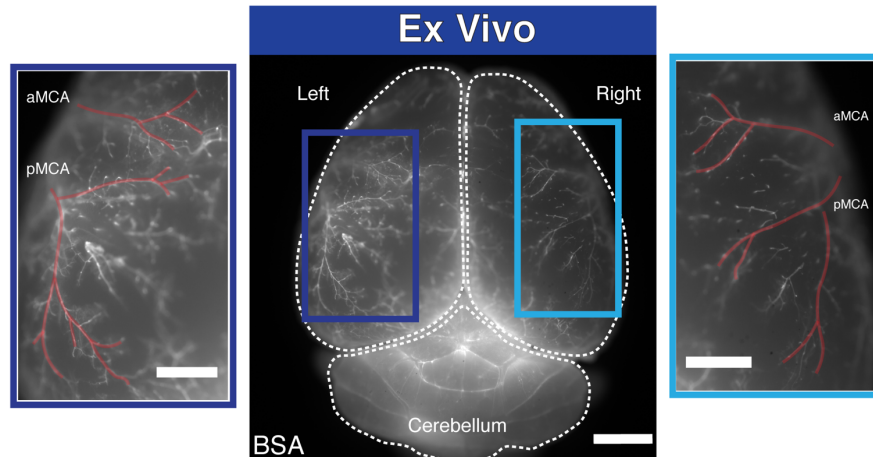
Anesthetized mice received cisterna magna (CM) injections of BSA-647 (BSA) during in vivo imaging and brains were extracted and fixed at 5-minute intervals between 5 and 30 minutes after the start of the infusion ( $n=3$  mice/6 time points). **(A)** Tracer transport color-coded as a function of time after CM injection in sagittal and coronal projections. **(B)** Coronal sections from the 5, 15, and 30 min time point after CM injection showing that tracer was transported from the base of the brain along the lateral cortical curvature, reaching the dorsal convexity in the later time points (scale bar = 2 mm). **(C)** Mean pixel intensity (MPI) of the last frame from transcranial in vivo imaging correlated with the MPI of 6 coronal sections from the same brain across all 6 time points (Pearson correlation,  $P = 0.0003$ ). **(D)** MPI has similar kinetics when quantified both in vivo and ex vivo and both data sets have good agreement with a one phase exponential decay function (in vivo:  $R^2 = 0.838$ ; ex vivo:  $R^2 = 0.834$ ). **(E)** To estimate the depth of tracer, MPI in arbitrary units (A.U.) was quantified in 1 mm ROIs starting from the dorsal cortex for all time points. The presence of tracer was determined as MPI values 2 standard deviations above background (dashed line). **(F)** The estimated distance of tracer below the dorsal cortex after the start of the intracisternal injection. Error bars reflect the 1 mm wide region of interest. Data was also fit with a one phase exponential decay ( $R^2 = 0.976$ ). **(G)** In vivo, ex vivo and tracer depth from (D) and (F), respectively, were z-score transformed and fit with a one phase exponential decay function. Extra sum-of-squares F test concluded that all three datasets were fit by a single global model and did not differ significantly ( $P = 0.288$ ;  $R^2 = 0.913$ ) suggesting that the increase in MPI on transcranial optical imaging is correlated with the tracer moving from the base of the brain towards the dorsal cortex. Data demonstrates that fluorescence is detected as early as 5 min after CM injection, when the bulk of tracer is located 5-6 mm below the cortical surface, providing great sensitivity for whole-brain tracer quantification comparable to terminal ex vivo methods



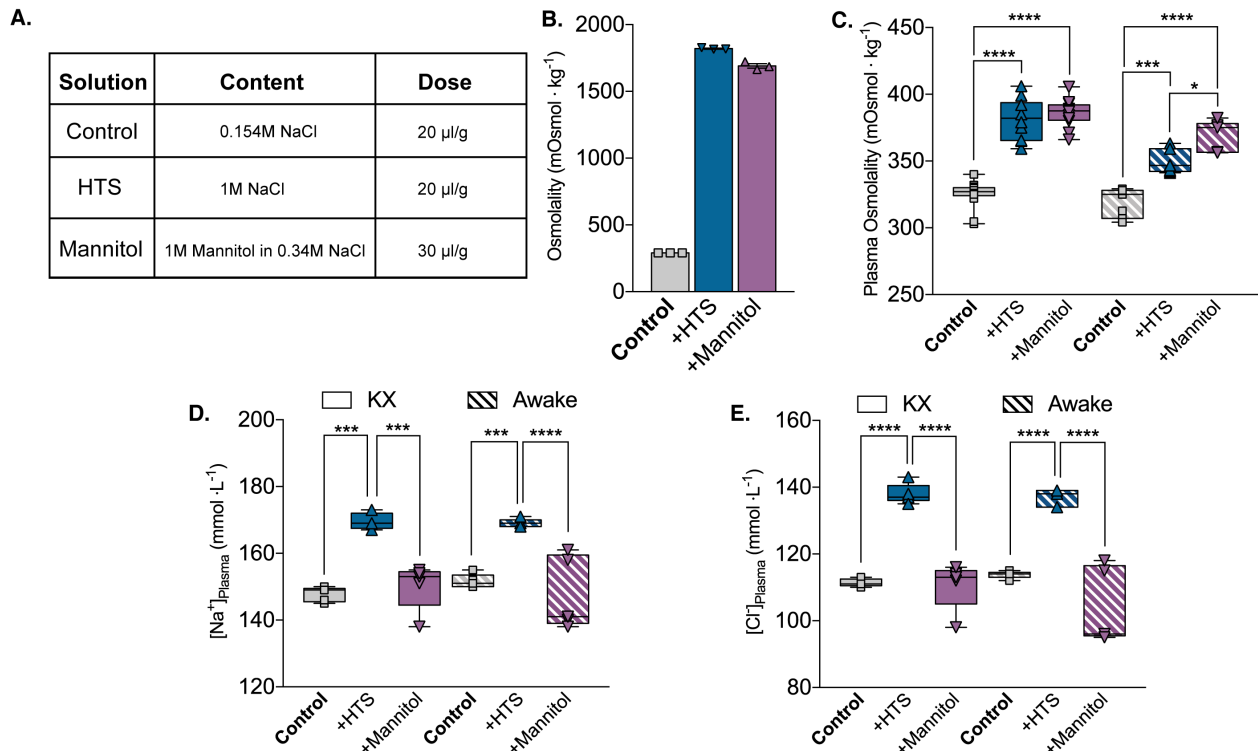
**Supplementary Figure 4. CSF tracer influx seen in transcranial imaging occurs along perivascular spaces surrounding arteries and has similar kinetics to previous *in vivo* imaging modalities. (A)** Macroscopic image from a typical experiment showing brain-wide CSF tracer (BSA-647) influx along the distribution of both middle cerebral arteries (MCA) after intracisternal injection (scale bar = 2 mm). **(B)** To evaluate the anatomical pathway along which CSF inflow occurs, a separate group of mice were imaged through a cranial window using two-photon laser scanning microscopy after intracisternal injection of BSA-Texas Red (TxRd) and i.v. FITC dextran to label vasculature (scale bar = 50  $\mu\text{m}$ ). The dura mater was left intact and the cranial window was sealed with agarose and a cover slip to prevent intracranial pressure loss. Imaging showed tracer flowing along two perivascular spaces (PVS) on each side of the MCA, below blood vessels of the dura (arrows). **(C)** Magnified image from inset in (A) shows CSF tracer on each side of the left posterior branch of the MCA (scale bar = 500  $\mu\text{m}$ ). **(D)** A line scan from the black line in (C) shows high pixel intensity (PI) in arbitrary units (A.U.) on both sides of the MCA with a decrease in fluorescence over the artery. The width of the space measured in (D) is comparable to that seen in (B). **(E)** Orthogonal reconstructions from the blue line in (B) shows that CSF tracer is confined to the subpial PVS around the MCA and not within the subarachnoid space (SAS; scale bar = 50  $\mu\text{m}$ ). **(F)** Quantification from the mean of 3 perivascular regions of interest along the MCA normalized to the maximum fluorescence intensity ( $\Delta F/F_{\text{max}}$ ) of the imaging session expressed as a percent. Higher baseline background fluorescence is seen in 2-P due to bleed through from the vascular label channel. **(G)** Time to tracer appearance after the start of the intracisternal injections. (mean  $\pm$  SEM; n = 4-5 mice/group; ns: not significant; unpaired t-test;  $P=0.8761$ ).



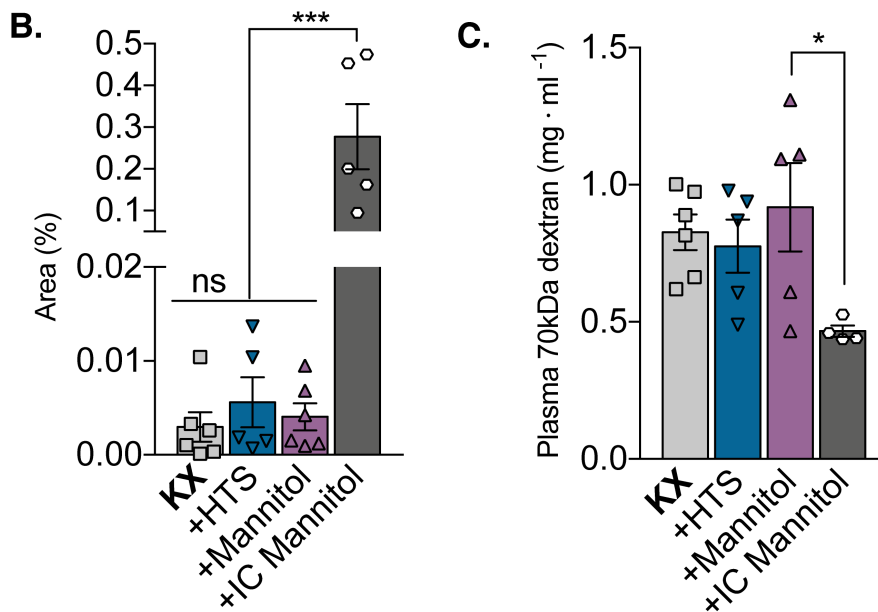
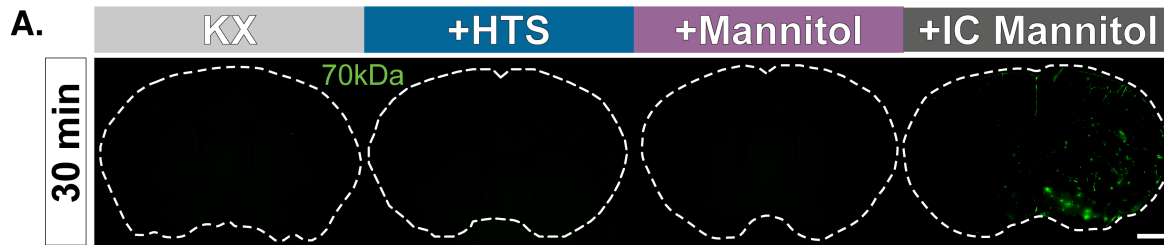
**Supplementary Figure 5. Transcranial macroscopic imaging of CSF influx pathways.** After tracer delivery into the cisterna magna it is possible to identify several intracranial structures through the intact skull (dashed line). (**Top panel**) In anesthetized mice, meningeal structures such as the olfactory sinus, superior sagittal sinus, and the left and right transverse sinuses can be observed (blue). As previously shown, tracer is first found in the large pools of subarachnoid CSF surrounding the brain like those around the olfactory cistern (purple) and the pineal recess (green). Brain uptake of the tracer occurs within the perivascular spaces of pial arteries (red), particularly following the distribution of the anterior and dorsal cortical segments of the middle cerebral artery, and then continues down into the brain along penetrating arteries. Eventually the tracer can be found in the perivenous spaces of the cortical bridging veins and surrounding the meningeal sinuses. (**Bottom panel**) In awake mice, some of the most anterior and posterior structures are covered by the headplate but all pial perivascular spaces can be readily identified. This approach can also be used for chronic imaging as it is still possible to identify tracer fluxes through transparent dental cement as can be seen on the edges of the headplate.



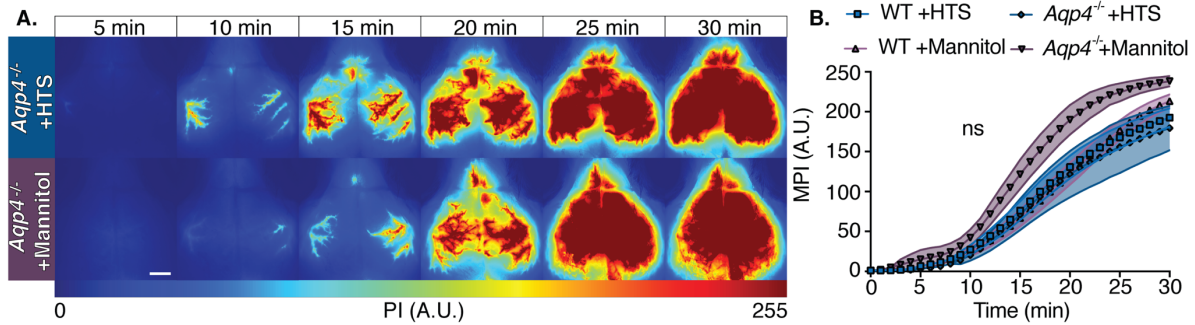
**Supplementary Figure 6. CSF tracer inflow routes imaged through the intact skull are also found in the ex vivo brain. (Center)** Ex vivo whole brain imaging from an anesthetized mouse, 30 minutes after intracisternal injection (scale bar = 2 mm). **(Left)** Higher magnification insets from the left cortical surface (dark blue) showing that CSF tracers can be found along branches of the anterior middle cerebral artery (aMCA) and posterior MCA (pMCA), traced in red (scale bar = 1 mm). **(Right)** Insets from the right cortex (light blue) demonstrating that tracer influx occurs along the same segments of the aMCA and pMCA (red traces; scale bar = 1 mm).



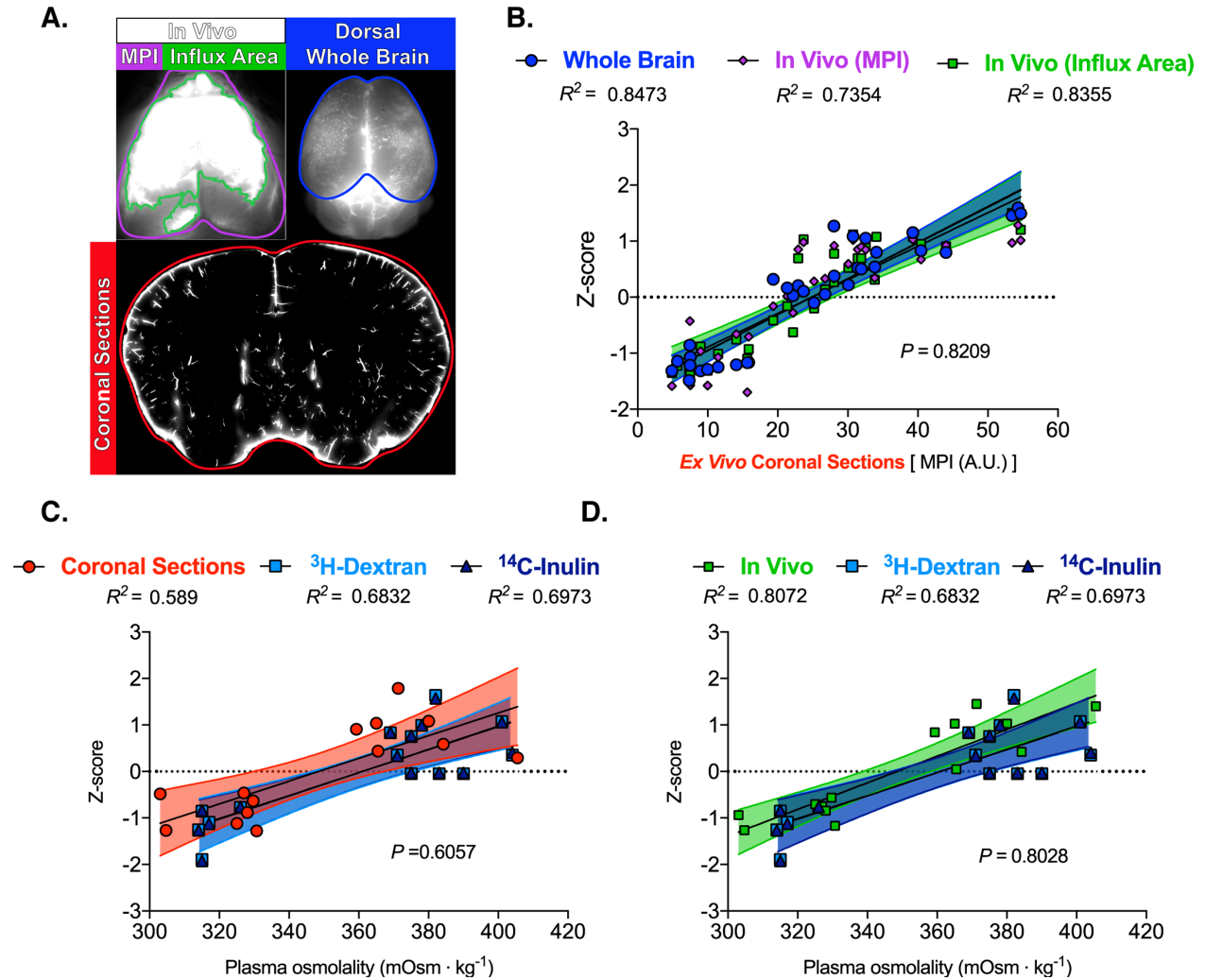
**Supplementary Figure 7. Inducing plasma hyperosmolarity.** (A) Solutions composition and dose used throughout the study. (B) Measured osmolality of plasma tonicity-shifting solutions. (C) Plasma osmolality at 30 minutes after intraperitoneal injection in the control, +HTS, and +Mannitol groups for both the anesthetized (KX) and awake conditions (mean  $\pm$  SEM;  $n = 5-15$  mice/group; ordinary two-way ANOVA, Tukey's multiple comparisons test; \* $P=0.0151$ , \*\*\* $P=0.0001$ , \*\*\*\* $P<0.0001$ ). (D) Plasma  $\text{Na}^+$  ( $[\text{Na}^+]_{\text{Plasma}}$ ) and (E)  $\text{Cl}^-$  ( $[\text{Cl}^-]_{\text{Plasma}}$ ) concentration 30 min after i.p. injection. High  $[\text{Na}^+]_{\text{Plasma}}$  and  $[\text{Cl}^-]_{\text{Plasma}}$  in the +HTS groups account for the hyperosmolarity seen in (c). Mannitol-induced plasma hyperosmolarity does not affect  $[\text{Na}^+]_{\text{Plasma}}$  and  $[\text{Cl}^-]_{\text{Plasma}}$  and is produced by an elevated osmolal gap. (mean  $\pm$  SEM;  $n = 5$  mice/group; ordinary two-way ANOVA, Tukey's multiple comparisons test; \*\*\* $P<0.001$ , \*\*\*\* $P<0.0001$ ).



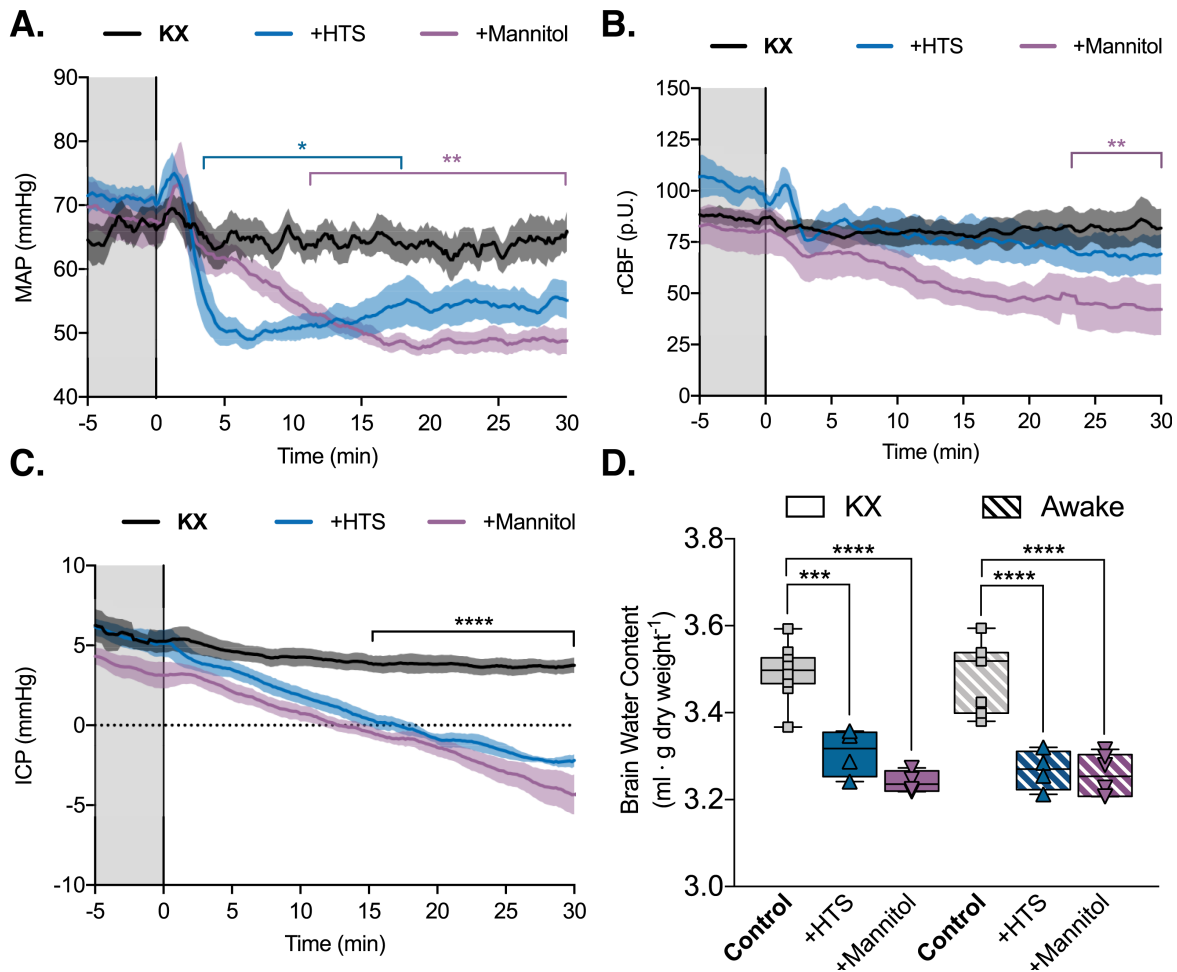
**Supplementary Figure 8. Manipulations of plasma tonicity do not disrupt the blood-brain barrier.** (A) Representative ex vivo coronal section images of FITC-dextran (1% m/v, 70 kDa) extravasation 30 minutes following intraperitoneal isotonic saline (KX), hypertonic saline (+HTS), and hypertonic mannitol (+Mannitol) solution administration in anesthetized animals. Positive controls received intracarotid 2M mannitol (+IC Mannitol). (scale bar = 1 mm). (B) Quantification of thresholded fluorescence expressed as percent area from 6 coronal sections depicted in (A) revealed no significant increases in extravasated FITC-dextran between the experimental groups but did show a significant difference between the experimental groups and the positive control, (mean  $\pm$  SEM;  $n = 5-6$  mice/group; one-way ANOVA, Tukey's multiple comparisons test, ns: not significant,  $P > 0.999$ ;  $***P < 0.0002$ ). (C) Plasma concentration of the FITC-dextran was evaluated spectrophotometrically and revealed no significant differences between any of the experimental groups but did show increased extravasation of the dextran in the positive control group (mean  $\pm$  SEM;  $n = 5-6$  mice/group; one-way ANOVA, Tukey's multiple comparisons test,  $*P = 0.0426$ ).



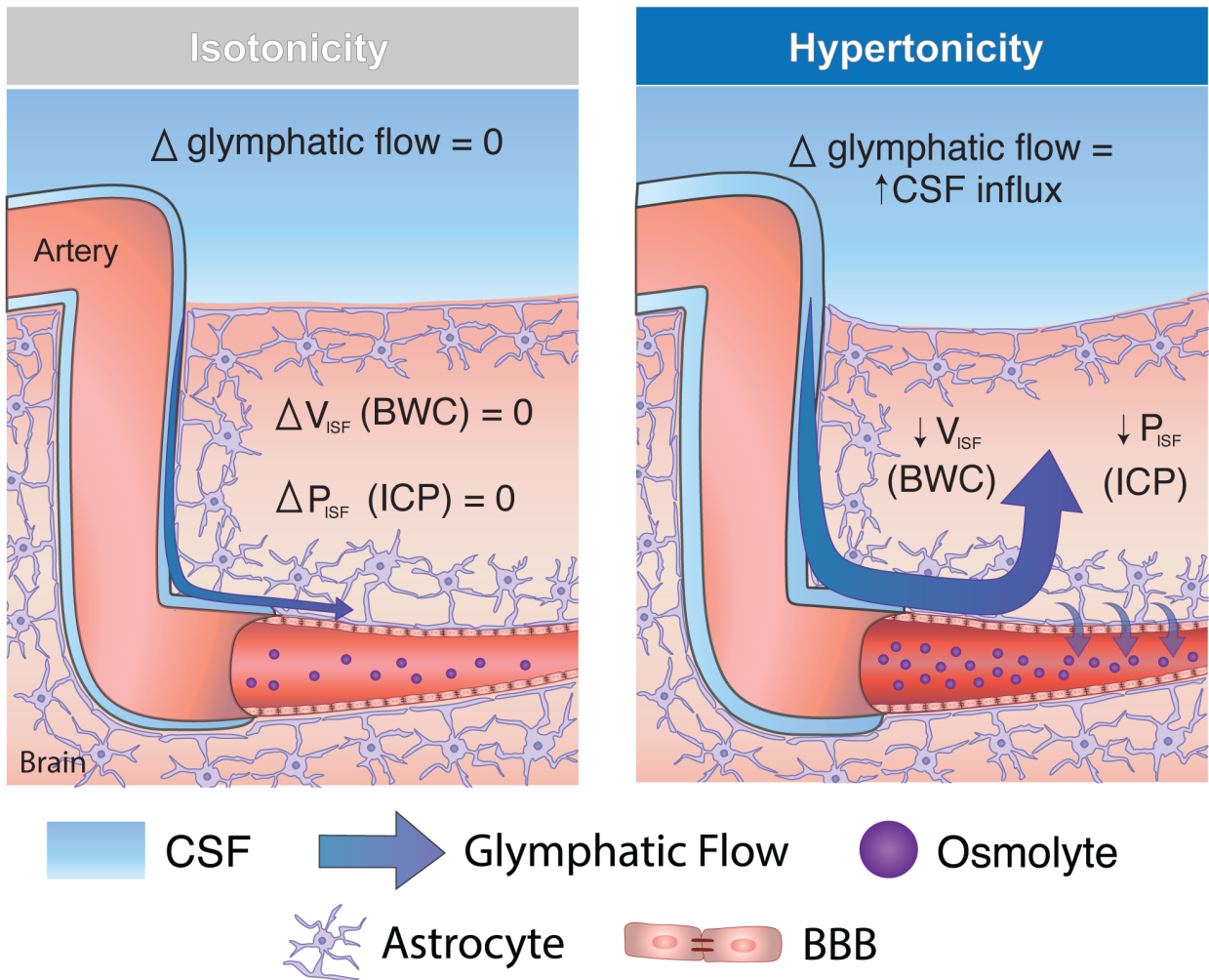
**Supplementary Figure 9. Plasma hypertonicity overrides glymphatic inhibition in *Aqp4*<sup>-/-</sup> mice.** Fluorescent BSA-647 was delivered into the cisterna magna (CM) of anesthetized *Aqp4*<sup>-/-</sup> mice. Mice received either hypertonic saline (*Aqp4*<sup>-/-</sup>+HTS), or hypertonic mannitol (*Aqp4*<sup>-/-</sup>+Mannitol) i.p. at the onset of the CM injection. **(A)** Representative time-lapse images of BSA-647 influx over the immediate 30 minutes following CM injection in the *Aqp4*<sup>-/-</sup>+HTS, and *Aqp4*<sup>-/-</sup>+Mannitol groups. Images (8-bit pixel depth, 0-255) are color-coded to depict pixel intensity (PI) in arbitrary units (A.U.). Scale bar = 2 mm. **(B)** Quantification of the mean pixel intensity (MPI) over time compared to the wildtype groups from Figure 2 (WT+HTS, WT+Mannitol; mean ± SEM; n = 3-5 mice/group; repeated measures two-way ANOVA, Sidak's multiple comparisons test; group effect:  $P=0.1029$ ; ns: not significant).



**Supplementary Figure 10. In vivo transcranial imaging correlates with ex vivo quantification of fluorescent and radio-labeled tracers.** (A) Images acquired at 30 min after in vivo imaging were analyzed for mean pixel intensity (MPI; purple) and influx area using front-tracking software (green). Mice were fixed and images of the dorsal whole brain (blue) and coronal sections (red) were acquired from the same brain using the macroscope. (B) Z-scores were calculated for all outcomes and a multiple linear regression model was generated from the data and plotted with 95% confidence intervals. All metrics had a significant positive linear relationship and were strongly correlated with ex vivo coronal sections (Whole Brain:  $R^2=0.8473$ ; In Vivo MPI:  $R^2=0.7354$ ; In Vivo Influx Area:  $R^2 = 0.8355$ ). The slopes of all three regressions were not significantly different from each other ( $P=0.8209$ ). Fluorescent tracer quantification from (C) ex vivo coronal sections and (D) in vivo imaging (influx area) was also tightly correlated with quantification of two separate radiotracers:  $^3\text{H-dextran}$  (40kDa) and  $^{14}\text{C-inulin}$  (6kDa) using plasma osmolality as the predictor (Coronal sections:  $R^2=0.589$ ; In Vivo:  $R^2=0.8072$ ;  $^3\text{H-Dextran}$ :  $R^2 = 0.6832$ ;  $^{14}\text{C-Inulin}$ :  $R^2 = 0.6973$ ). The overall slopes of all regressions were not significantly different ( $P>0.05$ ).



**Supplementary Figure 11. Plasma hyperosmolarity causes a decrease in intracranial pressure and interstitial fluid volume without altering mean arterial blood pressure or cerebral blood flow.** (A) Mean arterial blood pressure (MAP) in the femoral artery of anesthetized mice (KX) was recorded in mmHg, starting 5 min before i.p. injection of isotonic saline (Control), hypertonic saline (+HTS), and hypertonic mannitol solution (+Mannitol), for 30 minutes (mean  $\pm$  SEM  $n = 4-5$  mice/group; repeated measures two-way ANOVA, Tukey's multiple comparisons test;  $**P < 0.01$ , color-coded asterisks denote a difference between KX and +HTS or KX and +Mannitol at different time points). (B) Relative cerebral blood flow (rCBF; pressure units, p.U.) was measured using laser Doppler flowmetry (mean  $\pm$  SEM;  $n = 3-5$  mice/group; repeated measures two-way ANOVA, Tukey's multiple comparisons test;  $**P < 0.01$ , color-coded asterisks denote a difference between KX and +Mannitol at different time points). (C) Intracranial pressure (ICP) recording for the 5 minutes prior to and 30 minutes following i.p. injection at 0 minutes (mean  $\pm$  SEM;  $n = 4-5$  mice/group; repeated measures two-way ANOVA, Tukey's multiple comparisons test;  $****P < 0.0001$ ). (D) Brain water content at 30 minutes following i.p. injection in the control and hypertonic groups (mean  $\pm$  SEM;  $n = 4-10$  mice/group; ordinary two-way ANOVA, Tukey's multiple comparisons test;  $***P = 0.0001$ ,  $****P < 0.0001$ ).



**Supplementary Figure 12. Three-compartment model of the relationship between blood plasma, brain, and CSF under isotonic and hypertonic conditions.** In the situation of an isotonic blood plasma, there is no change in interstitial fluid volume ( $V_{\text{ISF}}$ ; brain water content, BWC) or pressure ( $P_{\text{ISF}}$ ; intracranial pressure, ICP), and as a result there is no change in the net direction or magnitude of glymphatic flow. In the hypertonic condition, with increased plasma osmolyte content there will be a net resorption of ISF, resulting in decreased ISF volume, and a negative ISF pressure that will enhance CSF influx into brain.

**Supplementary Video 1. In vivo transcranial imaging recapitulates the influence of sleep-wake states and AQP4 on CSF influx to brain.** (Left) Representative time-lapse imaging of an anesthetized (KX), (Center) awake, and anesthetized *Aqp4*<sup>-/-</sup> mouse (KX-*Aqp4*<sup>-/-</sup>) (Right). Fluorescent BSA-647 was delivered intracisternally at the beginning of the imaging session. Images were acquired every minute over 30 minutes and are color-coded for pixel intensity (0-255) as seen in Fig. 1c (scale bar = 2 mm).

**Supplementary Video 2. Front-tracking of CSF tracers through the intact skull.** (Left) Representative time-lapse imaging of an anesthetized mouse receiving fluorescent CSF tracer into the cisterna magna. The tracked tracer front generated from the front-tracking software has been overlaid. (Right) Tracked fronts are superimposed with time indicated by color-coding. These fronts were used to obtain both the area and the speed of CSF influx as seen in Fig. 1e-g (scale bar = 2 mm).

**Supplementary Video 3. Plasma hypertonicity causes a global increase in CSF tracer entry to the brain of anesthetized mice.** (Left) Representative time-lapse imaging of an anesthetized mouse (KX) that received i.p. isotonic saline, (Center) an anesthetized mouse that received i.p. hypertonic saline (+HTS), and (Right) an anesthetized mouse that received i.p. hypertonic mannitol (+Mannitol). Fluorescent BSA-647 was delivered intracisternally at the beginning of the imaging session. Images were acquired every minute over 30 minutes and are color-coded for pixel intensity (0-255) as seen in Fig. 2b (scale bar = 2 mm).

**Supplementary Video 4. Plasma hypertonicity enables the delivery of CSF tracers to the awake brain.** (Left) Representative time-lapse imaging of an awake headplated mouse (Awake) that received i.p. isotonic saline, (Center) an awake mouse that received i.p. hypertonic saline (+HTS), and (Right) an awake mouse that received i.p. hypertonic mannitol (+Mannitol). Fluorescent BSA-647 was delivered intracisternally at the beginning of the imaging session. Images were acquired every minute over 30 minutes and are color-coded for pixel intensity (0-255) as seen in Fig. 3b (scale bar = 2 mm).